Biophysical Journal
Article

Biophysical Society

Cholesterol catalyzes unfolding in membrane-inserted motifs of the pore forming protein cytolysin A

Avijeet Kulshrestha,[1] Sudeep N. Punnathanam,[1] Rahul Roy,[1,2] and K. Ganapathy Ayappa[1,*]
[1]Department of Chemical Engineering, Indian Institute of Science, Bangalore, Karnataka, India and [2]Center for BioSystems Science and Engineering, Indian Institute of Science, Bangalore, Karnataka, India

ABSTRACT Plasma membrane-induced protein folding and conformational transitions play a central role in cellular homeostasis. Several transmembrane proteins are folded in the complex lipid milieu to acquire a specific structure and function. Bacterial pore forming toxins (PFTs) are proteins expressed by a large class of pathogenic bacteria that exploit the plasma membrane environment to efficiently undergo secondary structure changes, oligomerize, and form transmembrane pores. Unregulated pore formation causes ion imbalance, leading to cell death and infection. Determining the free energy landscape of these membrane-driven-driven transitions remains a challenging problem. Although cholesterol recognition is required for lytic activity of several proteins in the PFT family of toxins, the regulatory role of cholesterol for the α-PFT, cytolysin A expressed by *Escherichia coli* remains unexplained. In a recent free energy computation, we showed that the β tongue, a critical membrane-inserted motif of the ClyA toxin, has an on-pathway partially unfolded intermediate that refolds into the helix-turn-helix motif of the pore state. To understand the molecular role played by cholesterol, we carry out string-method-based computations in membranes devoid of cholesterol, which reveals an increase of $\sim$30 times in the free energy barrier for the loss of β sheet secondary structure when compared with membranes containing cholesterol. Specifically, the tyrosine-cholesterol interaction was found to be critical to creating the unfolded intermediate. Cholesterol also increases the packing and hydrophobicity of the bilayer, resulting in enhanced interactions of the bound protein before complete membrane insertion. Our study illustrates that cholesterol is critical to catalyzing and stabilizing the membrane-inserted unfolded state of the β tongue motif of ClyA, opening up fresh insights into cholesterol-assisted unfolding of membrane proteins.

SIGNIFICANCE Cholesterol, an integral part of mammalian cell membranes, is necessary for activity of many pathogenic toxins. Our understanding of the thermodynamic and molecular underpinnings of cholesterol-protein interactions during different stages of toxin activity is unclear. Using path-based all-atom molecular dynamics simulations, we illustrate lowered free energy barriers and enhanced stability of the membrane unfolded intermediate of an α pore forming toxin (PFT) ClyA, providing insights into the increased pore-formation kinetics with cholesterol. Thus, membrane cholesterol, generally believed to have a passive receptor function for PFT activity, is involved in a more complex regulatory role in assisting secondary structure transitions critical to PFT lytic activity. Our findings could aid in drug development strategies for mitigating PFT-mediated bacterial infections.

INTRODUCTION

The environment of the plasma membrane plays a vital regulatory role in stabilizing membrane proteins important for cellular homeostasis (1). Transmembrane proteins are predominantly α-helical in structure and include the G-protein family of receptors (GPCRs), ion channels, and aquaporins (2). The translocon-mediated mechanism for protein insertion and folding in the plasma membrane has been widely investigated and provides a cotranslational pathway for protein synthesis and refolding in the phospholipid membrane (3). In contrast, pathogenic bacteria have evolved to express pore forming proteins (pore forming toxins [PFTs]) that form large transmembrane pore complexes on the plasma membrane using efficient membrane binding, as well as unfolding and refolding events of membrane-inserted motifs (4–6). The

Submitted May 7, 2023, and accepted for publication September 13, 2023.
*Correspondence: ayappa@iisc.ac.in
Editor: Chris Neale.
https://doi.org/10.1016/j.bpj.2023.09.005

process of oligomerization to form the oligomeric pore complex is often accompanied by large conformational changes that occur at the lipid interface. Since conformational changes and folding occur spontaneously in the membrane, studying the transition of pore forming proteins from a water-soluble monomeric state to the membrane-inserted protomer is expected to provide several insights into membrane-driven folding of proteins.

PFTs are a pathogenic class of the family of pore forming proteins that are expressed by bacteria to mount infections mediated by membrane-assisted assembly and pore formation (6). Pore formation allows the passage of crucial cellular components of different sizes ranging from ions to ATP molecules leading to cell death. Pores also provide passage to other proteins known as lethal factors to promote infections. PFTs are classified based on the secondary structure of the transmembrane region, which is α-helical for the α-PFTs and β barrels for the β-PFTs (5). In this study, we focus on cytolysin A (ClyA), expressed by *Escherichia coli*, *Salmonella typhi*, and *Shigella flexneri* (6). ClyA is a 34-kDa α-PFT that shows one of the largest conformational changes in PFTs, oligomerizing into a dodecameric pore state on the membrane. ClyA has more recently been the subject of investigation because of the availability of high-resolution crystal structures (7,8) of the monomer (Fig. 1 *A*) and the protomer states (Fig. 1 *B*). The major conformational changes that occur in ClyA during the transition from the monomer to the protomer states are the flipping out of the N terminus from the α-helical bundle and the conversion of β tongue to the helix-turn-helix motif as illustrated in Fig. 1. Using molecular dynamics (MD) simulations with structure-based models (SBMs), the monomer to protomer transition was shown to be triggered by the interaction of the predominantly hydrophobic β tongue motif with the membrane (9), confirming the original hypothesis postulated during the crystal structure elucidation of ClyA (8).

Determining the free energy associated with protein secondary structure changes in membranes requires a higher dimensional collective variable space to account for both membrane penetration-associated secondary structure changes as well as the protein orientation in some cases. Including the membrane and solvent extends the computational complexity involved in computing the free energy for large PFT proteins and secondary structure changes associated with pore formation. We recently developed a path-based method that can be used to efficiently evaluate free energy changes associated with membrane proteins (10). Using string-method-based free energy computations (10) and MD simulations in a 1-palmitoyl-2-oleoyl-sn-glycero-3-phosphocholine:cholesterol (POPC:Chol) (70:30) membrane,

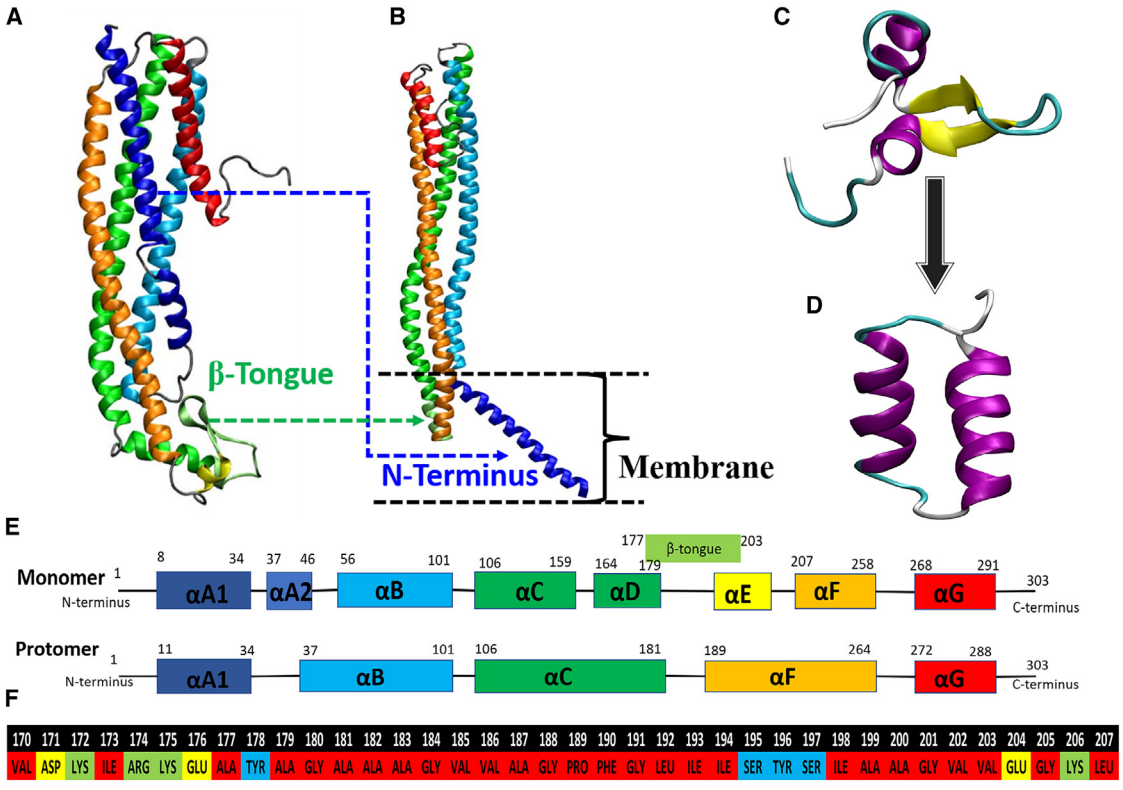

FIGURE 1 Cytolysin A structure detail. (*A*) Water-soluble monomer structure, (*B*) membrane-inserted protomer structure, (*C*) β tongue structure (170–207), (*D*) helix-turn-helix motif (170–207) of protomer state, (*E*) secondary structure detail of monomer and the protomer states, and (*F*) sequence of the amino acid residues of the truncated β tongue region used in free energy computations; red, non-polar; blue, polar; green, positively charged; yellow, negatively charged. Adapted from Kulshrestha et al. (4). Copyright 2023, American Chemical Society.

we have shown (4) that the transition of the membrane-inserted β tongue to the helix-turn-helix motif of the protomer state takes places through a partially unfolded intermediate. This transition to the unfolded state is spontaneous, and the refolding to the helix-turn-helix motif was shown to have a barrier of $\sim$26.56 kJ mol^{-1}. We further showed that single point mutations that lowered the flexibility of the β tongue motif resulted in impaired kinetics of pore formation, indicating that the inherent flexibility was critical to membrane-induced refolding and effective pore formation.

Cholesterol is a component of the mammalian cell membrane and several PFTs, such as listeriolysin O (LLO) and pneumolysin (PLY), which belong to the class of cholesterol dependent cytolysins (CDCs), code specificity into targeting cells by using cholesterol as a receptor (11–14). Although ClyA is not part of the CDC family of toxins, it has been shown to have higher pore forming and lytic activity in the presence of cholesterol (15,16). In a combined single molecule and simulation study in our laboratory, we showed that cholesterol plays a significant role in enhancing the pore forming activity of ClyA (17) and stabilized the pore complex by binding into pockets formed by adjacent β tongues of the pore complex. Whether cholesterol plays a role in membrane binding and/or assists the refolding of the β tongue is an important question with broad implications for other membrane protein folding transitions. To obtain a deeper understanding of the putative role of cholesterol, we study the nature of the folding intermediate for the β tongue and its presence in membranes devoid of cholesterol and make a detailed comparison with free energy computations reported earlier for membranes containing cholesterol (4).

Our study reveals a large free energy barrier associated with the unfolding transition of the β tongue in a POPC membrane devoid of cholesterol. This barrier is about 30 times greater than the barrier observed with cholesterol where partial unfolding occurred spontaneously. Tyrosine, known to be associated with anchoring proteins at the lipid aqueous interface, was shown to be a strong cholesterol binding motif that catalyzes the unfolding in the membrane. In the absence of cholesterol, reduced insertion of the β tongue is observed and the unbiased simulations reveal increased curvature and thinning of the POPC membrane consistent with the higher free energy associated with the transition in the absence of cholesterol.

MATERIALS AND METHODS

The crystal structure of the ClyA monomer was taken from the PDB: 1QOY (7) (see Fig. 1 *A*), and the crystal structure of the protomer state was taken from the PDB: 2WCD (8) (see Fig. 1 *B*). The β tongue (Fig. 1 *C*) and the helix-turn-helix motif (Fig. 1 *D*) were truncated from the monomer and the protomer state, respectively. The amino acid sequence and the residues (170–207) are shown in Fig. 1 *F*. We initially worked with the crystal structure definition of the β tongue (i.e., residue 177–203); however, the selected residues did not anchor to the membrane headgroups and lack certain charged residues. PFTs are known to have an evolutionary design in such a way that the charged residues reside at the edges of the transmembrane region, keeping the protein hinged to the lipid headgroup using electrostatic interactions (18,19). In the case of the ClyA, the β tongue region lies from residue 177 to 203 in the monomer, which does not have any charged residues; however, a few additional residues on both sides of the peptide have several charged residues (Fig. 1 *F*). Previously, the protomer simulations of the ClyA embedded in the membrane have shown additional residue interaction with the membrane components (17,20). Therefore, for our study, we consider residues from 170 to 207 of the β tongue, which were shown to interact with the membrane in the protomeric state, and their RKWY type of amino acid residues have electrostatic interaction with the lipid headgroup.

The initial structure of the bilayer was generated using the CHARMM-GUI membrane builder (21). Subsequently, initial structures of β tongue exposed to the membrane, β tongue placed in the membrane, and the helix-turn-helix motif placed in the membrane were prepared. For the membrane-exposed simulations, the protein center of mass (COM) was placed $\sim$2 nm above the phosphate atoms of the upper leaflet for both POPC and POPC:Chol membranes, where the distance was computed using the minimal distance between the protein COM and phosphate atoms of lipid membrane. All-atom MD simulations for the membrane-inserted and membrane-exposed truncated β tongue of monomer (Fig. 1 *C*) and the membrane-inserted truncated helix-turn-helix motif (Fig. 1 *D*) of the protomer state were performed on a POPC membrane and a POPC membrane with 30% cholesterol (POPC:Chol) similar to the composition used in supported bilayer experiments in the single molecule study by Sathyanarayana et al. (17). All initial structures were solvated with TIP3P water and Na^+ and Cl^- ions were added to maintain the charge neutrality and 150 mM physiological salt concentration. Initial solvated structures were energy minimized using the steepest-descent method with a maximal force of 1000 kJ mol^{-1} nm^{-1}. The energy minimized structures were then gradually heated up to 310 K, followed by 10 ns of NVT simulation and 20 ns of NPT simulations with position restraints on protein, lipid, and cholesterol molecules. The final configurations from the equilibration simulation were used as the starting structures for the production runs.

All simulations were performed in the NPT ensemble at 310 K using GROMACS-2018.6 with the force-field parameters for the ClyA protein taken from AMBER99SB-ILDFN force field with phi corrections, and the force-field parameters for lipid and cholesterol were taken from the compatible Slipids force fields (22–24). This force-field combination has been shown to accurately reproduce the crystal structure of dodecameric pore complex in the membrane environment and compared well with other force fields, such as the CHARMM36 protein and lipid force fields as well as the AMBER class of force fields (20,25). The semi-isotropic pressure control was achieved using the Parrinello-Rahman method with a time constant of 1 ps. The temperature was controlled using Nosé-Hoover chains with a time constant of 0.1 ps. The long range electrostatic interactions were treated using the particle mesh Ewald (PME) method with a real space cutoff of 1.5 nm and van der Waals interactions computed with a cutoff of 1.5 nm as recommended in the work by Jämbeck and Lyubartsev (24,26,27) where 1.4 and 1.5 nm were used for the electrostatic and van der Waals cutoff's respectively. With these cutoff values, the combination of AMBER99SB-ILDN and Slipid were found to yield good agreement with experimental properties of protein-membrane systems. Our choice of the cutoffs is based on the recommendations provided in this study. However, since the AMBER force fields were parameterized with a 1.0 nm van der Waals cutoff, we also extended our simulations of the converged string with the original 1.0 nm cutoff for both the van der Waal and real-space electrostatics. These simulations showed that the free energy values along the strings were insensitive to the different cutoff parameters and the variations were well within the statistical uncertainties of $\sim kT$. Three-dimensional periodic boundary conditions were applied to eliminate edge effects. Hydrogen bonds were constrained using the LINCS constraint, which allowed a larger time step of 2 fs (28). The solvent, lipid, cholesterol, and protein molecules were coupled separately to a temperature bath at 310 K.

Pressure was kept constant at 1 bar using the isothermal compressibilities, $K_{xy} = K_z = 4.5 \times 10^{-5}$ bar^{-1} (29). Equilibration was monitored by evaluating the root-mean-square deviation (RMSD) and secondary structure changes of the protein. Complete simulation details are given in Table S1.

String method simulation details

Two stable endpoints of the string were carefully selected based on the multiple replicates of the equilibrium simulations of membrane-inserted monomer and protomer states. For the POPC membrane, the two endpoints are the β sheet (Fig. S3 *A*) and the helix-turn-helix motif (Fig. S3 *B*). This is in contrast to simulations with cholesterol where we observed spontaneous unfolding of the β tongue and hence used the partially unfolded state as one of the endpoints of the string (4). The conformation phase space was defined using path collective variables (PCVs) (S, Z) originally developed by Branduardi et al. (30). The PCVs defined for a system consist of N number of atoms with positions $(\mathbf{r}_1, \mathbf{r}_2, \ldots, \mathbf{r}_N) \equiv \mathbf{R}$ undergoing a conformational change. First, we consider a sequence of n reference structures $\{\mathbf{R}^{(1)}, \mathbf{R}^{(2)}, \ldots, \mathbf{R}^{(n)}\}$ of the molecule under consideration, connecting two endpoints of the conformational change. With the help of reference structures, PCVs are defined as

$$S(\mathbf{R}) = \frac{\sum_{i=1}^{n} i e^{-\lambda D\left(\mathbf{R}^{(i)}, \mathbf{R}\right)}}{\sum_{i=1}^{n} e^{-\lambda D\left(\mathbf{R}^{(i)}, \mathbf{R}\right)}} \quad (1)$$

and

$$Z(\mathbf{R}) = -\frac{1}{\lambda} \ln\left(\sum_{i=1}^{n} e^{-\lambda D\left(\mathbf{R}^{(i)}, \mathbf{R}\right)}\right) \quad (2)$$

where S denotes the progress from one endpoint to the other along the reference path, and Z is a measure of the variation in the perpendicular direction. In our work, the reference path consisting of 20 states for the PCVs was generated using linear interpolation between the atomic coordinates of the structures between the two end states. The λ values were 594.88 nm^{-2} for the POPC:Chol membrane and 422.00 nm^{-2} for the POPC membrane. These values are inversely proportional to the mean square displacement (MSD) between two consecutive states on the reference path.

Sampling from the unbiased simulations of the endpoints projected in (S, Z) space is shown in Fig. S3 *C* for the POPC membrane where the states are clearly distinguishable and indicate the presence of a free energy barrier. The string was defined by 50 points connecting the initial and final states. To evolve the string, a force constant of 100 kJ mol^{-1} was used in the S and Z variables. During string evolution, 0.5 ns of simulations were performed on each point in every iteration until the string converged. The convergence of the string was monitored using

$$C = \frac{1}{P} \sum_{j=1}^{P} \|\boldsymbol{\theta}_j^{(k+1)} - \boldsymbol{\theta}_j^{(k)}\| \quad (3)$$

where, $\boldsymbol{\theta}_j$ represents the coordinates (S_j, Z_j) and $\|\cdot\|$ is the Euclidian norm. The superscript k is the iteration number, subscript j represents the point on the string, and P is the total number of points on the string. The string converged in 12 iterations for the POPC membranes (see Fig. S3 *D*). Additional 60 ns umbrella sampling simulations on each point of the converged path were performed to obtain a converged free energy landscape along the transition path. The overlapping of histograms for the weighted histogram analysis method (WHAM) analysis was ensured by examining the regions with sampling counts greater than 0.1 million as illustrated in Fig. S3 *F*. The 1D free energy profile was reported on the arc length parameterized distance P calculated from the monomer state to the protomer distance. The convergence of the free energy profile was monitored using the evolution of the free energy profile upon performing additional simulations at each point along the string. In Fig. S3 *E*, the free energy was found to be invariant beyond 45 ns of simulation.

Simulation analysis

Gromacs in-built commands were used to compute RMSD, root-mean-square fluctuation (RMSF), and the radius of gyration. Time trajectories of secondary structure changes were monitored using Gromacs "do-dssp" command and visual molecular dynamics (VMD) timeline features with the structural identification method (STRIDE) software. For the Chol and POPC atom-atom occupancy analysis with the protein, contact between two atoms was assumed to occur if the distance was less than a cutoff distance of 0.5 nm (31,32).

The fractional occupancy O_r for residue, r is defined using

$$O_r = \frac{1}{LT} \sum_{t=1}^{T} \sum_{l=1}^{L} C_{t,l}^{r} \quad (4)$$

where t is the time index, T is the total simulation time, l is the index for number of lipid molecules, and L is the total number of lipid molecules. $C_{t,l}^{r}$ denotes the total number of contacts formed between r^{th} residue and l^{th} lipid molecule at time t and is evaluated using

$$C_{t,l}^{r} = \sum_{i=1}^{R_a} \sum_{j=1}^{L_a} \left(1 - H\left(r_{i,j} - r_{cut}\right)\right) \quad (5)$$

where $H(x - x_o)$ is the Heaviside step function whose values is 0 when $x < x_o$ and 1 when $x \geq x_o$. R_a is the number of atoms in the protein residue and L_a is the number of atoms in a cholesterol molecule. The occupancy values were further normalized with the maximal occupancy value.

The membrane curvature and the thickness were computed using the MDAnalysis Python package (33), where, first, a reference group of atoms is selected to define the upper and lower membrane surfaces. We have chosen phosphorous atoms of upper and lower leaflets to define the respective surfaces. Every atom of the reference group is assigned a grid based on its x and y location. Once every grid is populated with the reference atoms, the z coordinates of the atoms are stored for each configuration. The average upper and lower surfaces were reported by averaging each grid value. The difference between the lower and upper leaflet surfaces was used to compute the membrane thickness, and the mean curvature was evaluated using the method proposed by Yesylevskyy and Ramseyer (34). The extent of penetration of the protein or residue in the membrane is carried out by analyzing the z coordinate of the distance between the COM of the protein/residue and the COM of the membrane.

RESULTS AND DISCUSSION

Cholesterol promotes the unfolding of β tongue monomer state

We first carry out MD simulations to study the secondary structure changes of the β tongue in POPC and POPC:Chol membranes (Fig. 2). These simulations are required to determine the end states of the protein for the string-method-based free energy computations. Unlike in the case of POPC:Chol membranes (4) where the protein partially unfolds and the β sheet content is completely lost (Fig. 2 *C*), the structure of the β tongue remained stable without appreciable loss of β sheet content (Fig. 2 *B*) in the absence of cholesterol. However, in both cases, the β tongue remained hinged to the lipid headgroups.

The average behavior of the RMSD from three independent MD simulations (Fig. 2 *D*) shows a higher RMSD of

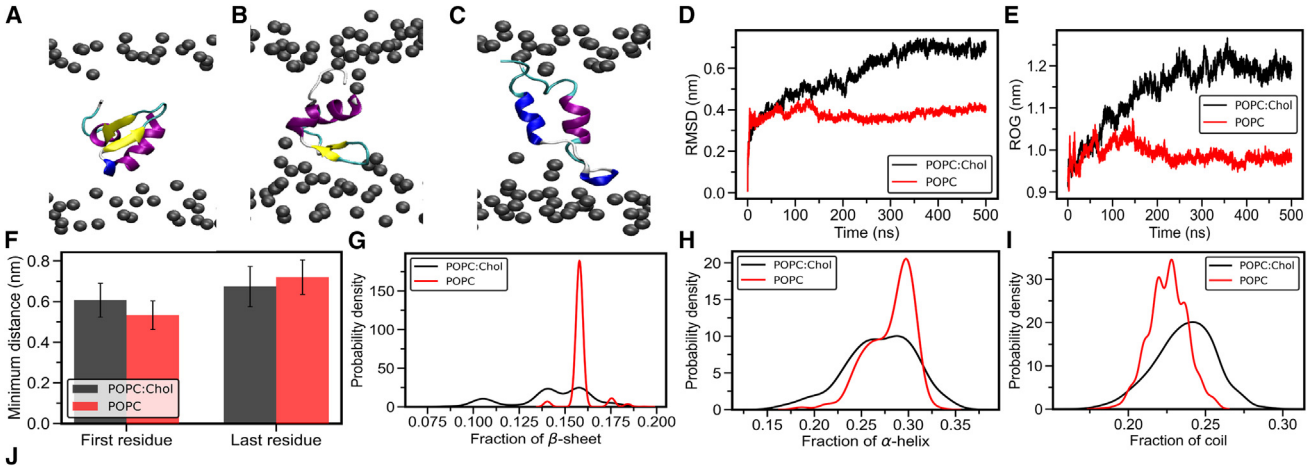

J

Residue	170 VAL	171 ASP	172 LYS	173 ILE	174 ARG	175 LYS	176 GLU	177 ALA	178 TYR	179 ALA	180 GLY	181 ALA	182 ALA	183 ALA	184 GLY	185 VAL	186 VAL	187 ALA	188 GLY	189 PRO	190 PHE	191 GLY	192 LEU	193 ILE	194 ILE	195 SER	196 TYR	197 SER	198 ILE	199 ALA	200 ALA	201 GLY	202 VAL	203 VAL	204 GLU	205 GLY	206 LYS	207 LEU
Monomer β-tongue Crystal	C	H	H	H	H	H	H	H	H	H	T	T	T	T	T	E	E	E	C	G	G	G	C	E	E	E	H	H	H	H	T	T	S	S	T	T	C	C
Monomer β-tongue (POPC:Chol)	C	C	S	H	H	H	H	S	H	H	H	H	H	G	G	G	C	C	C	G	G	G	C	C	C	C	G	G	G	G	G	G	G	C	S	S	C	C
Monomer β-tongue (POPC)	C	C	S	C	H	H	H	H	H	H	H	H	H	H	T	E	E	E	C	G	G	G	C	E	E	E	H	H	H	H	H	T	C	S	S	S	C	C
Protomer helix-turn-helix Crystal	C	H	H	H	H	H	H	H	H	H	H	H	G	G	G	G	S	S	C	H	H	H	H	H	H	H	H	I	I	I	I	I	H	H	H	H	T	C
Protomer helix-turn-helix (POPC:Chol)	C	H	H	H	H	H	H	H	H	G	G	G	C	C	T	T	T	H	H	H	H	H	H	H	H	H	H	H	H	H	H	H	H	H	C	S	C	C
Protomer helix-turn-helix (POPC)	C	C	T	T	T	H	H	H	H	H	H	H	H	T	T	T	C	C	S	T	T	H	H	H	H	H	H	H	H	H	H	H	T	T	T	T	T	C

FIGURE 2 Monomer β tongue placed in the membrane. (*A*) Initial state of the β tongue placed in the membrane. The final structure of the β tongue at the end of the 500-ns simulation for the (*B*) POPC membrane and (*C*) POPC:Chol membrane. (*D*) Average RMSD and (*E*) average radius of gyration (ROG) comparison for POPC:
Chol and POPC membrane averaged over three independent 500-ns simulations. (*F*) The minimal distance between the C-α atom of the first (170) and last residue (207) to the lipid headgroups. Fraction of secondary structure content for (*G*) β sheet, (*H*) α helix, and (*I*) coil structure. (*J*) Residue-wise (red, nonpolar; blue, polar; green, positively charged; yellow, negatively charged) secondary structure in crystal structures and different membrane environments. Color and string codes are as follows: pink, α helix (*H*); teal, turn (*T*); yellow, β sheet (*E*); blue, 3_{10}-helix (*G*); red, π helix (*I*); green, bend (*S*); white, coil (*C*). RMSD and ROG data for POPC:Chol adapted from Kulshrestha et al. (4). Copyright 2023, American Chemical Society.

around 0.7 nm for the POPC:Chol membrane and 0.4 nm for the POPC membrane after 300 ns of the simulation. The radius of gyration (Fig. 2 *E*) also suggests that the protein remains more compact in the POPC membrane with a lower value of radius of gyration. To quantify the hinged state of the protein as illustrated in Fig. 2 *B* and *C*, we evaluated the averaged minimal distance between the Cα atom of the first (VAL170) and last (LEU207) residues of the β tongue with the phosphorous atoms of the lipids (Fig. 2 *F*). The data illustrate that both the terminal residues are in close proximity to the lipid head groups independent of the presence of cholesterol. Once hinged, they remain attached to the headgroup with a distance of around 0.5–0.6 nm for the first residue (VAL) and 0.6–0.7 nm for the last residue (LEU). Both of these are adjacent to charged residues ASP171, LYS172, and LYS206, which can form electrostatic interactions with the lipid headgroups to stabilize these hinged configurations. These electrostatic interactions play a broader role across membrane proteins and residues such as ARG, LYS, TRP, and TYR have been shown to stabilize protein interactions in the headgroup region at the protein-membrane interfaces in pores formed by ClyA and α-hemolysin (19).

The fraction of secondary structure content (Fig. 2 *G–I*) also indicates a distinct unfolding of the β sheet in the presence of cholesterol where increased conversion into a coil structure is observed. In contrast, the secondary structure content is more rigid in the absence of cholesterol and this tendency is the greatest in the case of the β sheet (Fig. 2 *G*). The representative differences in the secondary structure content for the β tongue residues are summarized in Fig. 2 *J* for configurations taken at the end of a single 0.5-μs simulation. For the monomer β tongue in the POPC:Chol membrane, we observe an increase in 3_{10} helices (G) and coils (C) with a complete absence of β sheets (E) when compared with the crystal structure. In contrast, the β tongue in POPC retains a similar secondary structure to the crystal state. In the POPC membrane, the resistance of the β tongue to unfold suggests the presence of a barrier to form the partially unfolded intermediate state and hence to refold to the helix-turn-helix motif of the protomer state. Since we are interested in capturing the mechanism for the conformational

change, we select the β tongue state (Fig. 2 *B*) as one endpoint of the string for the free energy analysis in the POPC membrane. We note that, in earlier free energy computations in the POPC:Chol membrane, a partially unfolded state was used as one endpoint for the free energy analysis since this state was formed spontaneously in the MD simulations.

To define the second end state of the string for the free energy analysis, we simulated the helix-turn-helix motif (residues 170–207) of the protomer, which is the stable conformation of the membrane-inserted pore state, placed in the POPC:Chol and POPC membranes (Fig. S1). The protomer state in both membranes remained stable and was found to be hinged to the lipid headgroups as illustrated in Fig. S1 *F*. These simulations indicate that the helix-turn-helix motifs are stable conformations that could be used as endpoints for the string method analysis. The secondary structure analysis (Fig. 2 *J*) also revealed that the helix-turn-helix motifs for the protomer states are preserved in both membranes.

We next apply the string method to capture the transition from the β sheet state (Fig. 2 *C*) to a protomer state (Fig. S1 *B*) in the POPC membrane and use a similar method based on PCVs (30) as outlined in our previous work (4).

Unfolding of β tongue is the on-pathway intermediate of the conformational change

In Fig. 3 *A* and *B*, we illustrate the converged paths obtained from the string method analysis for the POPC and POPC:Chol membranes respectively. To facilitate a comparison between the two membranes, we adapted the free energy data from our previous work and computed several additional properties to quantify the changes along the string for the POPC:Chol membrane (4). The converged strings to the transition path for both cases remain below 0.2 nm^2 in Z, indicating that the transition path does not deviate significantly from the reference path defined at $Z = 0$. In case of the POPC:Chol membrane, the initial state at $S = 1$ corresponds to the partially unfolded state, and $S = 20$ corresponds to the final protomer state. For the POPC membrane, $S = 1$ corresponds to the β sheet state of the monomer in the POPC membrane as determined from unrestrained MD simulations discussed earlier. Representative snapshots of the structures on the converged path are shown in Fig. 3. These structures were generated using additional short biased MD simulations for 3 ns using harmonic potentials for S and Z with 1000 kJ mol^{-1} nm^{-1} spring constants. For all points sampled along the path, we observe that N (green) and C (red) terminals remain hinged to the lipid headgroups for both membranes. For the POPC membrane, we also observe large deviations in the phospholipid headgroups from a planar configuration. The influence of the protein on the topological changes to the membrane surface is quantified and discussed later in the text.

An analysis of the secondary structure changes on the converged path along the string is shown in Fig. 3 *C* with the corresponding free energy profiles in Fig. 3 *D*. A detailed stride analysis of the secondary structure evolution for the final configurations on the converged string is given in the Fig. S4. In the POPC membrane, the β sheet content is

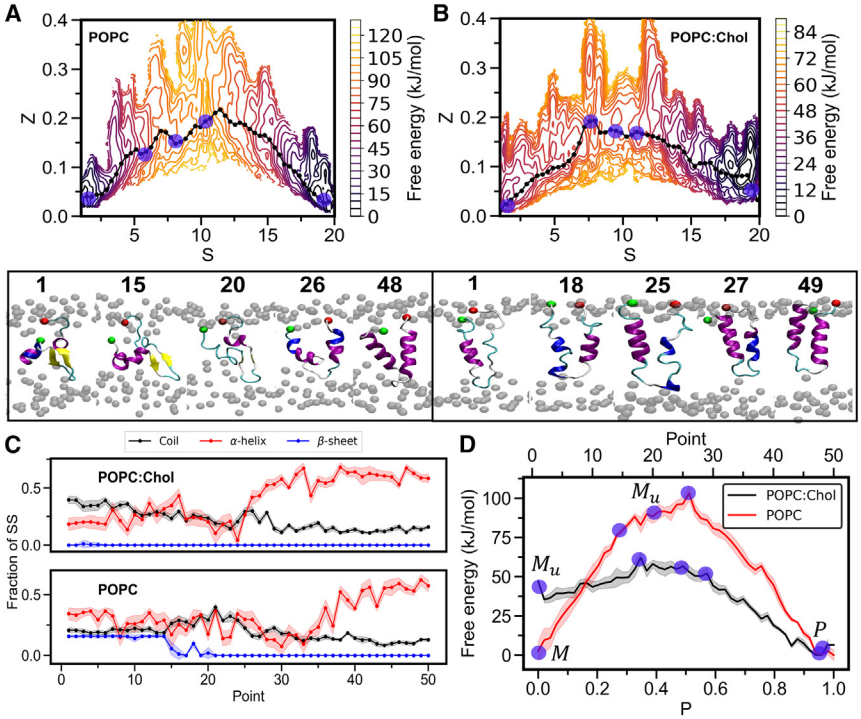

FIGURE 3 Transition path of ClyA β tongue and the free energy profile. The final converged string (black color) and the free energy surface contour plot for the case of (*A*) the transition from the β tongue to the protomer state in POPC membrane, and (*B*) the transition from the unfolded state to the protomer state in the membrane with cholesterol. A few representative snapshots of the structure on the path are shown below, where the green sphere represents the N terminus and the red sphere represents the C terminus. The values of (S, Z) for the corresponding point on the string are given in Tables S2 and S3 for POPC:Chol and POPC membrane, respectively. (*C*) Fraction of secondary structure changes on the transition path. (*D*) 1D free energy profile along the parameterized distance P calculated from partially unfolded state to the protomer state for POPC:Chol membrane and β sheet to protomer state for POPC membrane. Transparent blue circles in (*A*), (*B*), and (*D*) are the locations of the different snapshots. Free energy data in (*A*) and (*D*) for POPC:Chol adapted from Kulshrestha et al. (4). Copyright 2023, American Chemical Society.

lost between points 1 and 20 on the string, and an increase in the formation of turns is observed in this region. Reduced β sheet content is observed in the corresponding snapshot shown at point 15 and the free energy rises to about 80 kJ mol^{-1}at this point. Subsequently, we observe fluctuations in the helical content indicative of unfolding (see snapshot point 27) and a further rise in the free energy until it reaches a maximum at point 26. Finally, the C terminus strand gains helicity where it fluctuates between 3_{10} helix and α helix (Fig. S4) until it completely converts into an α helix. At later points, we observe a refolding to form the helix-turn-helix motif of the protomer and this is accompanied by a decrease in the free energy to the protomer state. Thus the primary barrier for the transition in the absence of cholesterol lies in the unfolding of the β sheet. Once unfolding is maximized, the refolding transition is downhill in the free energy profile. In case of the POPC:Chol membrane, secondary structure data along the points confirm the presence of a partially unfolding transition along the string; however, a weak barrier in the free energy that forms between points 20 and 30 is only $\sim$10 kJ mol^{-1}, reflecting the strong role played by cholesterol in spontaneously unfolding the β sheet. Refolding takes place beyond point 24 accompanied by a decrease in the free energy.

Cholesterol stabilizes the protomer state and enhances the kinetics of the conformational change

Fig. 3 *D* illustrates the differences in the free energy landscape for the POPC and POPC:Chol membranes. We propose the transition from monomer (M) to protomer (P) follows a two-step process passing through a partially unfolded monomer intermediate M_u.

$$M \rightarrow M_u \rightarrow P$$

Since the partially unfolded state M_u depleted of β sheet content in the POPC:Chol membrane was found to be a stable intermediate state, we ascribe the point on the string with the zero β sheet content to define the corresponding intermediate M_u for the POPC membrane, which occurs at point 20 on the string (Fig. 3 *C*) lying below the maximum in the free energy.

Tabulated values of the free energy changes are given in Table 1 where the barrier to form M_u from the M state ($\Delta G_1 = G_{M_u} - G_M$) in the POPC membrane is 85.55 kJ mol^{-1}. Since M_u forms spontaneously at room temperature for the POPC:Chol membrane, we assign the barrier to be of order k_BT. The free energy difference ($\Delta G_2 = G_P - G_{M_u}$) to transform from M_u to the protomer state is about three times lower for the POPC:Chol membrane. Upon closer inspection, the free energy profiles reveal that the protein from the M_u state must overcome a small barrier during the transformation to the helix-turn-helix protomer state. This barrier is associated with an additional loss of secondary structure due to a decrease in α-helical content and an increase in turns and 3_{10} helices (Figs. 3 *D* and S4). We evaluate the corresponding free energy change as the difference between the transition state, i.e., the maximum (point 26 for POPC and 18 for POPC:Chol) and the free energy of the M_u state ($\Delta G_3 = G_{max} - G_{M_u}$). The free energy barrier for this secondary transition is about a factor of two greater for the POPC:Chol membrane. Once this barrier is surmounted, refolding to the protomer state is a downhill process. Therefore, for the POPC membrane, the largest barrier occurs during the unfolding stage of the monomer in the membrane (ΔG_1). These barriers that we observe are related to the kinetics of the transitions that occur when the protein binds to the membrane. Our study with the β tongue motif sheds light on only one part of the conformational changes. The complete transition also involves the insertion of the N-terminal helix into the membrane (Fig. 1). We next draw qualitative connections with experiments carried out with ClyA with the present free energy analysis. The kinetics of pore formation vary widely depending on the specific membrane platform and assay used (17). In dye leakage experiments with small unilamellar vesicles, the leakage kinetics increased by a factor of three in the presence of cholesterol. Interestingly in POPC:Chol vesicles, the kinetics was invariant for cholesterol content ranging from 30% to 50% indicating the presence of a threshold cholesterol concentration for robust pore formation. In contrast, turbidity assay experiments with ClyA showed a 100-fold increase in rupture activity when cholesterol was present. These differences result in part from the large curvature present in the vesicle leakage experiments, which retard the pore formation kinetics. Despite these variations, our free energy computations indicate the lowered barrier in the presence of cholesterol consistent with the enhanced leakage kinetics observed in the experiments (17,35,36).

TABLE 1 Free energy data

Membrane	ΔG_1 kJ mol^{-1}	ΔG_2 kJ mol^{-1}	ΔG_3 kJ mol^{-1}
POPC	85.55 ± 10.9	−88.44 ± 7.9	14.66 ± 7.9
POPC:Chol	$\sim k_BT$	−35.43 ± 2.49	26.56 ± 5.30

Free energy differences ΔG are reported for transitions between the monomer M, protomer P, and partially unfolded monomer M_u states. Here, $\Delta G_1 = G_{M_u} - G_M$, $\Delta G_2 = G_P - G_{M_u}$, and $\Delta G_3 = G_{max} - G_{M_u}$.

Tyrosine and the unfolding transition with cholesterol

To obtain molecular insights into the role of cholesterol, we analyzed the structures and interactions along the transition path using several different metrics. In Fig. 4 *A*, the average cholesterol occupancy computed from the last 50 ns of the biased trajectory on the converged path indicates that Tyr178 has the greatest occupancy, followed by Arg174 in the initial points along the path. However, cholesterol interactions have a broader distribution across the residues along the path and, in the protomer state, several residues show

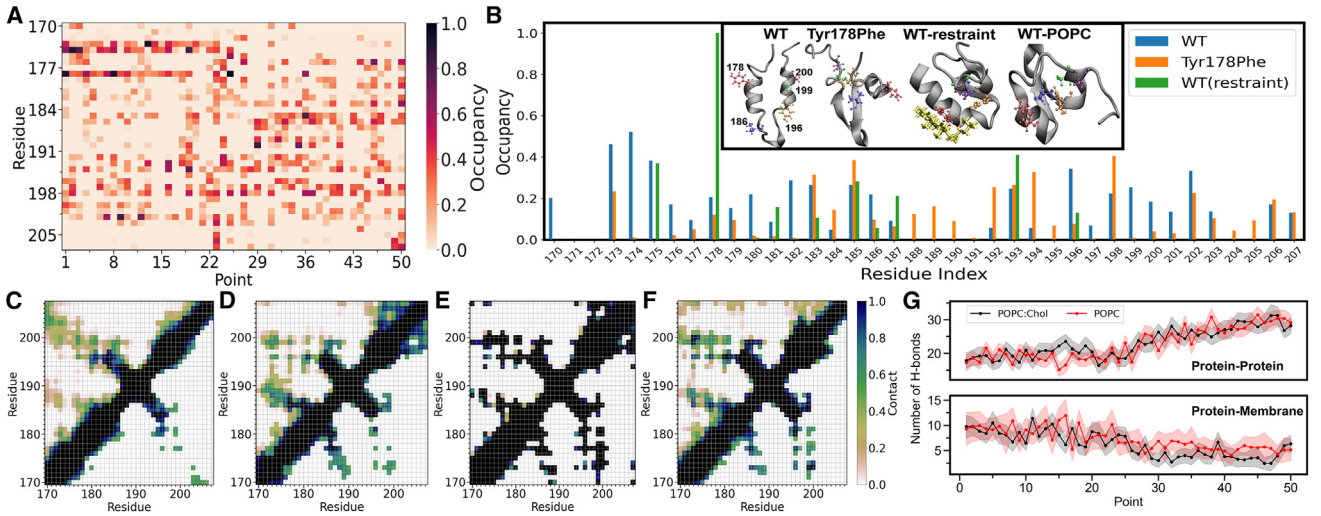

FIGURE 4 Conformational changes of the ClyA β tongue. (*A*) Average cholesterol occupancy comparison for each residue of monomer β sheet in POPC:Chol membrane on the transition path. (*B*) Residue-wise average cholesterol occupancy for wild type (WT) and Tyr178Phe mutant. Insets represent the snapshots taken at the end of the 500 ns MD simulations, where the residues 178, 186, 196, 199, and 200 are colored red, blue, orange, green, and purple, respectively. Cholesterol molecule interacting with restraint WT is shown in yellow color. Contact map of protein for (*C*) WT, (*D*) Y178F mutant, (*E*) WT restraint, and (*F*) WT in POPC membrane. Lower triangular regions of contact maps are plotted only for contact values greater than 0.5 to identify strong contacts. (*G*) The number of protein-protein and protein-membrane hydrogen bonds, for the POPC and POPC:Chol membranes.

strong cholesterol binding sites. These sites correspond to cholesterol hot spots observed by us earlier in simulations of the dodecameric ClyA pore complex in a POPC:Chol membrane (17) where cholesterol was found to bind between pockets formed by adjacent membrane-inserted β tongue motifs. In a recent mutagenesis and thermal unfolding study, we showed a near-complete abrogation of lytic activity of the mutant Tyr178Phe in erythrocyte turbidity and the vesicle leakage assays. Furthermore, this mutant was resistant to thermal unfolding in membranes containing cholesterol (4), revealing that conformational flexibility was an important factor in assisting secondary structure changes involved during ClyA pore formation. Since the Tyr178 was found to be a key residue (Fig. 4 *A*), we analyzed the β tongue, Tyr178Phe mutant trajectories from our earlier study (4) to compare the cholesterol occupancies (Fig. 4 *B*). Tyr178Phe showed significantly reduced cholesterol occupancy at residues 174 and 178; however, increased occupancy occurred at other residues of the β tongue. For comparison we also computed the cholesterol occupancy for the wild type (WT) β tongue with and without restraints to discern the differences between a folded and unfolded state, respectively, noting that the WT spontaneously unfolds in the presence of cholesterol. Tyr178 is clearly a cholesterol-binding hot spot when unfolding is prevented using a restraint. A snapshot from the simulation (see inset in Fig. 4 *B*) shows the binding of the α face of cholesterol with tyrosine. In the absence of restraints where the WT partially unfolds, cholesterol occupancy at Tyr178 is drastically reduced (Fig. 4 *B*). From this analysis, we hypothesize that cholesterol interaction with Tyr178 is critical to catalyzing the spontaneous unfolding of the β tongue and stabilizing the partially unfolded intermediate. This interaction is transient and occurs during the initial stages of unfolding. Evidence for this is discussed later in the text. Using replica exchange MD, Miller et al. (37) have shown that the presence of tyrosine in the cholesterol recognition and consensus (CRAC) motif of leukotoxin facilitates unfolding of the peptide, suggesting that the interaction with tyrosine, a necessary residue for the definition of the CRAC motif, is essential for this transition. We point out that the tyrosine present in the β sheet motif is not part of a CRAC motif implicated in cholesterol-protein interactions (38).

The contact maps of protein based on the distance between C_α atoms <1 nm (Fig. 4 *C–F*) reveals the role of cholesterol in the WT protein during β tongue unfolding. The lower triangular part of the contact maps only depicts strong contacts, defined as those that persist for greater than 50% of the simulation time. The contact map of the partially unfolded WT shows a loss of all strong contacts (Fig. 4 *C*) in comparison to the WT protein restrained to prevent unfolding (Fig. 4 *E*). In the case of the restrained WT, residue 178 makes strong contact with residues 186, 196, 199, and 200 (Fig. 4 *E*). WT ClyA in the POPC membrane (Fig. 4 *F*) largely retains the same strong contacts (between 178 residue and residues 186, 199, and 200), suggesting that cholesterol is involved in the unfolding observed in restraint free simulations. Similarly, Tyr178Phe mutant displays a comparable contact map in the vicinity of residue 178 with a strong contact with residue 186 (Fig. 4 *D*) providing additional evidence that Tyr178 is indeed necessary for cholesterol-mediated unfolding. Overall, our contact map

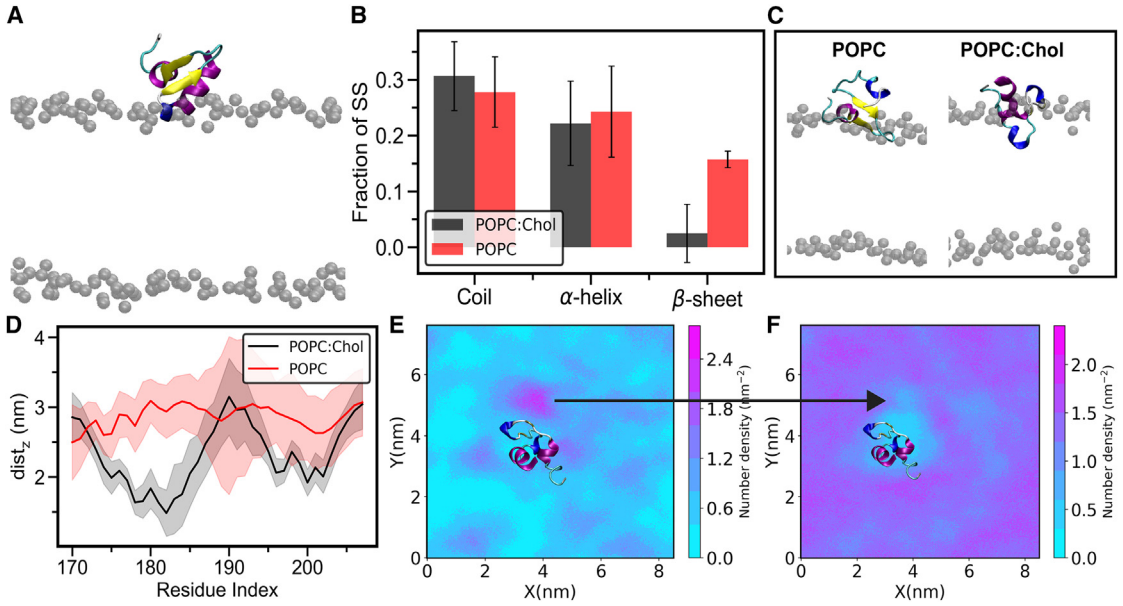

FIGURE 5 The β tongue exposed to the membrane. (*A*) Initial state of the β tongue exposed to the POPC:Chol and POPC membrane, with only the location of the phospholipid headgroups illustrated for clarity. (*B*) Fraction of secondary structure (SS) content. (*C*) Final snapshots of the protein in the membrane at the end of 1 μs long simulation. (*D*) Residue-wise depth analysis with the z coordinate of the distance between the COM of a residue and the COM of the membrane. Number density map for (*E*) cholesterol molecules and (*F*) POPC molecules in the upper leaflet of the POPC:Chol membrane system; the black arrow indicates the accumulation of the cholesterol near the protein and displacement of the POPC molecules.

analysis along with the occupancy analysis suggest that the Tyr178 has a strong affinity to interact with the α face of the cholesterol, and its interaction with cholesterol disrupts the internal contacts within the β tongue motif leading to the unfolded state with reduced contacts. Once the protein is unfolded, other residues are accessible to cholesterol but none reveal a strong propensity to outcompete the others (Fig. 4 *A*). Consistent with the idea that the major role of cholesterol is to induce unfolding, the occupancy at residues 174/178 disappears at point 19 (Fig. 4 *A*) concomitant with loss of α helix and β sheet content (Fig. 3 *C*).

The variations in the number of hydrogen bonds (H-bonds) between protein atoms and protein and membrane atoms are shown in Fig. 4 *G*. The number of protein-protein H-bonds remains ~20 until point 25 along the string for both the POPC and POPC:Chol membranes, with a subsequent increase associated with refolding to the protomer state. This refolding is found to occur around point 25 on the string for the POPC:Chol membrane and a little later for the POPC membrane (Fig. 3). However, we were unable to discern the differences in the H-bond data between the two membranes. Concomitant with the increase in H-bonds for the protein-protein interactions, we observe a decrease in protein-membrane H-bonds.

Cholesterol facilitates the β tongue insertion

The study has thus far focused on the conformational changes that occur when the β tongue is inserted in the membrane. However, it is also of interest to study the extent of secondary structure changes when the monomer first binds to the membrane. Since membrane binding is primarily mediated by the β tongue (20,8), we carried out two microsecond long replicates of MD simulations with the β tongue initially placed in the vicinity of the phospholipid headgroups for both POPC:Chol and POPC membranes (Fig. 5 *A*). In Fig. 5 *B*, the fraction of secondary structure analysis reveals a distinct loss of β sheet content in the presence of cholesterol in the membrane, consistent with the behavior observed when the β tongue was inserted into the membrane, reiterating that unfolding is on pathway to the conformational change accompanying the monomer to protomer transition. In the first simulation, the β sheet unfolds within 200 ns of simulations, and we did not observe any refolding events over the 1 μs timescale of our simulation; however, in a second set of simulations, β sheet content shows a higher fluctuation of folding and unfolding in the cholesterol containing membrane (see Fig. S5.) The final snapshots in Fig. 5 *C* illustrate an increased unfolding of the protein in the POPC:Chol membrane along with increased membrane penetration. Furthermore, residue wise depth analysis in Fig. 5 *D* indicates that the residues toward the N terminus lie deeper in the POPC:Chol membrane when compared with the POPC membrane. It is important to note that the N terminus side of the monomer consists of many charged residues (Fig. 1 *F*), which have enhanced cholesterol binding (Fig. 4 *A*).

We have also simulated the β tongue motif in solution to assess the protein stability in the absence cholesterol. In Fig. S2, the RMSD analysis indicates that the protein is well equilibrated within 200 ns of simulations, and the β sheet

remains stable as illustrated in Fig. S2 *B*. Interestingly, the helical region of the protein first unfolds and then converts into a β sheet, resulting in the increase in the β sheet secondary structure content. This observation further supports our view that the innate unfolding of the β sheet in the POPC:Chol membrane is catalyzed by the presence of cholesterol.

We analyze the redistribution of cholesterol and phospholipids around the protein using the 2D number density maps illustrated in Fig. 5 *E* and *F*, respectively. These data are computed from MD simulations where the β tongue is placed at the membrane interface (Fig. 5 *E*) and averaged over the last 500 ns of the 1 μs restraint free simulations. The number density reveals the enhanced density of cholesterol molecules around the protein, suggesting that preferential binding of cholesterol occurs before the complete insertion of the β tongue in the membrane playing a key role in facilitating the β tongue insertion as observed in the POPC:Chol membrane. We point out that MD simulations of the complete ClyA monomer placed at the phospholipid interface (4) with the β tongue in close proximity to the headgroups also showed the partial unfolding and insertion of the β tongue over a 1 μs simulation in the POPC:Chol membrane, indicating that these trends are generic and consistent with the trends observed with the isolated β tongue motif reported here.

To unambiguously confirm the critical role played by Tyr178 in our MD simulations is more complex. The focus on Tyr178 is primarily motivated from our single point mutation study where experiments revealed a complete loss of activity with the Tyr178Phe mutant (4). The cholesterol occupancy for the membrane-exposed β tongue simulations suggests that the stretch of residues between 177 and 188 predominantly participate in cholesterol binding, with Tyr178 showing the strong contact (see Fig. S6). A more detailed time series contact analysis from the membrane-exposed simulations also showed strong interactions of Tyr178 with cholesterol during the initial 200 ns of the simulation during which the β tongue motif was observed to unfold (see Fig. S5). However in the membrane-inserted partially unfolded state, cholesterol interactions are reduced, and, coupled with the experimental results and the restraint simulations (folded β tongue in POPC:Chol), lead us to conclude that Tyr178-cholesterol interactions are transient and important in the early stages of membrane binding, assisting the initial unfolding of the β tongue motif. The role of Tyr has also been implicated in the second membrane binding motif of ClyA (17) where Tyr present in the N terminus is part of a CRAC motif and a strong cholesterol binding site. Here again, a single point mutation of Tyr27Phe was found to completely abrogate pore formation, suggesting that Tyr-cholesterol interactions are perhaps more widespread and specific.

Membrane modulation with cholesterol

Using the mean position of the phosphate atoms for the upper and lower leaflets (Fig. 6), we examined the influence of different conformations of the β tongue motif on membrane thickness variations and ensuing deformations. The surface representations of the local membrane thickness are illustrated in Fig. 6 *A–D* for the initial monomer and final protomer states of the protein used for the string-method computations. Analysis of the curvature for different points along the string reveals similar differences between the two membranes. Cholesterol is known to increase the thickness of a POPC membrane (39) and we observe a similar increase in the thickness in our simulations. Additionally, the increase in the lipid tail order parameter for PC lipids in the presence of cholesterol has been well documented (40–42). In the presence of the β tongue, significant differences in the local membrane thickness variations are observed between the POPC and POPC:Chol membranes. The average thickness of the membrane with the protein reduced from 40.42 $\pm$ 0.53 nm to 36.57 $\pm$ 0.55 nm in the absence of cholesterol. In the POPC membrane, the presence of the protein results in large curvature and membrane thickness modulations across both leaflets of the membrane. The upper leaflet shows a large positive mean curvature (Fig. 6 *E*) with a corresponding negative mean curvature in the lower leaflet. Additionally, the local curvature and height variations are greatest in the vicinity of the protein (Fig. 6 *E*) and occur in both the monomer and protomer states (Fig. 6 *A–D*). In contrast, the membrane thickness and curvature variations in the POPC:Chol membranes are less; however, we observe smaller topological variations in the upper leaflet where the N and C termini are anchored. The increased free energy penalty due to larger induced curvature (43) in the membrane for the POPC bilayer is consistent with the higher free energy for the transition from the monomer to the protomer in the absence of cholesterol. Thus, the barrier for unfolding of the protein is also influenced by the extent of membrane deformation exacerbated in the absence of cholesterol. Proteins, especially curvature inducing proteins, have been found to remodel the membrane followed by preferential accumulation of curvature sensing proteins on the curved surface (44). Since cholesterol modulates membrane properties, it is natural to question whether the changes observed originate from the intrinsic role played by cholesterol or whether the modulated membrane properties are responsible for the increased activity of ClyA. We discuss this next.

Cholesterol has the smallest area in binary POPC:Chol membranes when compared with either DOPC or DPPC lipids, creating a closer packed arrangement of cholesterol (45). In addition to increasing the membrane thickness, cholesterol reduces the lipid volume by $\sim$15% for the POPC:Chol (70:30) membrane. These properties indicate that both lipids and cholesterol in the POPC:Chol membranes are tightly packed when compared with the POPC membrane devoid of cholesterol (45). Cholesterol increases the hydrophobicity at the bilayer center, decreasing it at the membrane interface, increasing the hydrophobic gradient

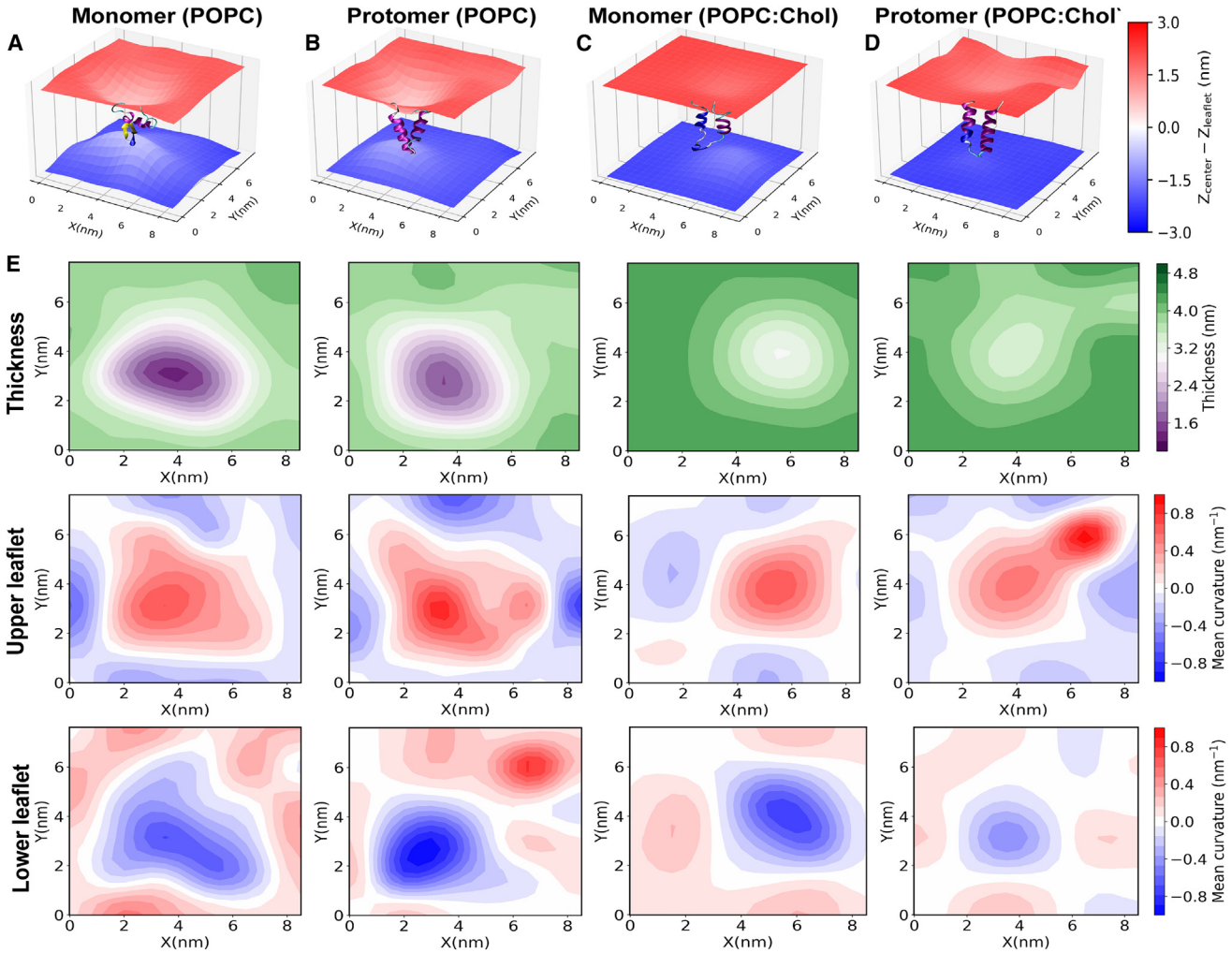

FIGURE 6 Membrane modulation. Upper extracellular and lower cytosolic leaflet mean surface representations for (*A*) monomer, (*B*) protomer placed in POPC membrane, (*C*) monomer, and (*D*) protomer placed in POPC:Chol membrane. z_{center} is the average z coordinate of the center of the membrane, and the $z_{leaflet}$ is the average surface coordinate of a leaflet. Red denotes the upper leaflet and blue denotes the lower leaflet surfaces. (*E*) Thickness and the upper and lower leaflet mean curvatures for POPC and POPC:Chol membranes.

across the bilayer (42). The net increase in hydrophobicity can be observed with decreased water penetration for the membrane-inserted protein configurations in the POPC:Chol membrane (see Fig. S7). Since the β tongue is predominantly hydrophobic (Fig. 1 *F*) in content, one would expect that the presence of cholesterol would enhance membrane binding and penetration of residues, as observed in Fig. 5 *D*. Indeed, upon analysis of the cholesterol occupancy for membrane-exposed β tongue simulations, we observed the stretch of residues between 177 and 188 to predominantly participate in cholesterol binding (see Fig. S6). This supports our earlier observations from MD simulations with SBMs where β tongue insertion events were enhanced with increased membrane hydrophobicity (9). In addition to model membrane systems where addition of cholesterol to POPC membranes increases ClyA pore forming activity, similar trends are observed with erythrocytes, which represent a more complex lipid and protein environment where removal of cholesterol has been shown to drastically reduce pore forming activity (17).

Although we cannot directly rule out the role of modified membrane properties due to the presence of cholesterol, such as the increased bulk modulus (46,47) and membrane thickness, our observations from MD simulations coupled with the experimental findings provide compelling evidence to suggest that cholesterol enhances interactions with the β tongue in the initial stages of binding. We note that our free energy analysis of the membrane-inserted folding transition reflects the collective state of the membrane modified with cholesterol.

CONCLUSIONS

The ClyA PFTs undergoes one of the largest conformational changes during membrane binding and pore formation. The predominantly hydrophobic β tongue motif inserts into the

membrane and undergoes a secondary structure transition to a helix-turn-helix motif. Kinetics of ClyA pore formation are known to be facilitated by cholesterol; however, the molecular underpinnings for this transition are poorly understood. Here, we report for the first time an extensive free energy analysis using the string method of the folding that occurs in the β tongue motif of ClyA in phospholipid membranes to unravel the specific role played by cholesterol in this transition. Our simulations reveal the presence of a large barrier for the β tongue to unfold in the absence of cholesterol, confirming that unfolding of this transmembrane pore motif is a critical step in the pore formation pathway of ClyA. Combined with our earlier work where we reported the free energy change for the β tongue in the presence of cholesterol (4), we posit that cholesterol catalyzes and stabilizes the unfolded intermediate, which subsequently refolds to complete the conformational change. Refolding to form the helix-turn-helix motif in both POPC and POPC:Chol membranes is a favorable downhill transition on the free energy path. Analysis of the secondary structure content along the path reveals that the β sheet structure is resistant to unfolding in the absence of cholesterol and spontaneously unfolds in the presence of cholesterol. More specifically, initial binding of cholesterol to the residue Tyr178 in the β tongue motif appears to trigger the unfolding in the membrane. This is consistent with the observation that a single point mutation Tyr178Phe was found to severely abrogate ClyA pore formation activity and MD simulations also showed the resistance to unfold in a POPC:Chol membrane (4) for this mutant. Therefore, cholesterol is able to compete for interactions with Tyr178 to interfere with its role in stabilizing the folded β tongue but is also fine tuned such that it no longer interferes in refolding after the structure has unfolded. The larger barrier to unfolding in the absence of cholesterol is accompanied by membrane topological deformations that result in increased membrane curvature and thinning.

A missing piece in our study is the insertion free energy of the β tongue into different membrane environments. Our results, however, point to the presence of a lowered barrier for membrane binding and insertion of the β tongue for the POPC:Chol membrane to result in the formation of a local unfolded intermediate in the presence of cholesterol. The free energy change associated with this initial step is outside the scope of the present work and would also require taking into consideration the membrane-inserted motif of the ClyA protein, which have been shown to couple to the partial unfolding observed in restraint free MD simulations of the full ClyA protein at the membrane interface (4).

It is well established that CDCs (12) use cholesterol molecules as their receptor. However, ClyA an α toxin that does not belong to the CDC family of toxins shows a higher activity in the presence of cholesterol. In an earlier MD simulation, cholesterol was found to bind to pockets formed by adjacent β tongue motifs, thereby stabilizing the dodecameric ClyA pore complex (17). In light of the findings in this work, we are able to provide a more complete story of the complex role played by cholesterol in the pore-formation pathway for ClyA. In addition to stabilizing the pore complex, cholesterol facilitates the initial unfolding of the β tongue, thereby lowering the barrier for the transition to the helix-turn-helix motif of the pore state. We argue that this is the primary driver for the enhanced pore formation and lysis kinetics observed in the presence of cholesterol (17). Although we have not carried out free energy computations of the initial β tongue binding, our restraint free MD simulations suggest that cholesterol triggers the loss of secondary structure during the initial binding stage, assisting in greater membrane penetration. In addition to the specific problem of secondary structure transformation for the ClyA PFTs, our findings suggest that cholesterol is a necessary ingredient for several active processes in the plasma membrane (48) and plays a critical role in secondary structure transitions and folding of proteins in a membrane environment. This binding step would also be influenced by membrane compositional changes such as the presence of anionic membrane lipids such as phosphatidylserine. Our study illustrates that path-based methods with appropriate collective variables provide an efficient and tractable means of computing the free energy associated with these transitions. The method can potentially be extended to study a wide class of membrane-protein folding events. We finally mention that monitoring the kinetics of protein folding in membranes is challenging, and our proposed pathway can potentially be confirmed with nuclear magnetic resonance (NMR) and circular dichroism techniques.

SUPPORTING MATERIAL

Supporting material can be found online at https://doi.org/10.1016/j.bpj.2023.09.005.

AUTHOR CONTRIBUTIONS

A.K., MD simulations, post-processing, data curation, interpretation, writing – original draft, writing – review & editing. S.N.P., R.R., and K.G.A., conceptualization, interpretation of results, and writing – review & editing.

ACKNOWLEDGMENTS

We acknowledge the Supercomputer Education and Research Center (SERC) computing facility; Thematic Unit of Excellence on Computational Materials Science (TUE-CMS), a Department of Science and Technology (DST)-supported computing facility at the Indian Institute of Science Bangalore; and the National Supercomputing Mission, India, for funding used in this work.

DECLARATION OF INTERESTS

The authors declare no competing interests.

REFERENCES

1. Blazek, A. D., B. J. Paleo, and N. Weisleder. 2015. Plasma membrane repair: a central process for maintaining cellular homeostasis. *Physiology.* 30:438–448.
2. Albers, R. W. W. 2012. Cell membrane structures and functions. *In* Basic Neurochemistry Elsevier, pp. 26–39.
3. Cymer, F., G. Von Heijne, and S. H. White. 2015. Mechanisms of integral membrane protein insertion and folding. *J. Mol. Biol.* 427:999–1022.
4. Kulshrestha, A., S. Maurya, …, K. G. Ayappa. 2023. Conformational flexibility is a key determinant of the lytic activity of the pore-forming protein, Cytolysin A. *J. Phys. Chem. B.* 127:69–84.
5. Dal Peraro, M., and F. G. Van Der Goot. 2016. Pore-forming toxins: ancient, but never really out of fashion. *Nat. Rev. Microbiol.* 14:77–92.
6. Bischofberger, M., I. Iacovache, and F. G. Van Der Goot. 2012. Pathogenic pore-forming proteins: function and host response. *Cell Host.* 12:266–275.
7. Wallace, A. J., T. J. Stillman, …, P. J. Artymiuk. 2000. E. coli hemolysin E (HlyE, ClyA, SheA): X-ray crystal structure of the toxin and observation of membrane pores by electron microscopy. *Cell.* 100:265–276.
8. Mueller, M., U. Grauschopf, …, N. Ban. 2009. The structure of a cytolytic α-helical toxin pore reveals its assembly mechanism. *Nature.* 459:726–730.
9. Giri Rao, V. V. H., R. Desikan, …, S. Gosavi. 2016. Capturing the membrane-triggered conformational transition of an α-helical pore-forming toxin. *J. Phys. Chem. B.* 120:12064–12078.
10. Kulshrestha, A., S. N. Punnathanam, and K. G. Ayappa. 2022. Finite temperature string method with umbrella sampling using path collective variables: application to secondary structure change in a protein. *Soft Matter.* 18:7593–7603.
11. Matsuzaki, K., K. Sugishita, …, K. Miyajima. 1995. Molecular basis for membrane selectivity of an antimicrobial peptide, magainin 2. *Biochemistry.* 34:3423–3429.
12. Tweten, R. K. 2005. Cholesterol-dependent cytolysins, a family of versatile pore-forming toxins. *Infect. Immun.* 73:6199–6209.
13. Gilbert, R. J. C. 2010. Cholesterol-dependent cytolysins. *Adv. Exp. Med. Biol.* 677:56–66.
14. Morton, C. J., M.-A. Sani, …, F. Separovic. 2019. Cholesterol-dependent cytolysins: membrane and protein structural requirements for pore formation: Focus review. *Chem. Rev.* 119:7721–7736.
15. Oscarsson, J., Y. Mizunoe, …, B. E. Uhlin. 1999. Molecular analysis of the cytolytic protein ClyA (SheA) from Escherichia coli. *Mol. Microbiol.* 32:1226–1238.
16. Sathyanarayana, P., S. S. Visweswariah, and K. G. Ayappa. 2021. Mechanistic insights into pore Formation by an α-Pore forming toxin: Protein and lipid bilayer interactions of cytolysin A. *Acc. Chem. Res.* 54:120–131, E7323–E7330.
17. Sathyanarayana, P., S. Maurya, …, R. Roy. 2018. Cholesterol promotes cytolysin A activity by stabilizing the intermediates during pore formation. *Proc. Natl. Acad. Sci. USA.* 115:E7323–E7330.
18. Tanaka, K., J. M. M. Caaveiro, …, K. Tsumoto. 2015. Structural basis for self-assembly of a cytolytic pore lined by protein and lipid. *Nat. Commun.* 6:6337–6411.
19. Varadarajan, V., R. Desikan, and K. G. Ayappa. 2020. Assessing the extent of the structural and dynamic modulation of membrane lipids due to pore forming toxins: insights from molecular dynamics simulations. *Soft Matter.* 16:4840–4857.
20. Desikan, R., P. K. Maiti, and K. G. Ayappa. 2017. Assessing the structure and stability of transmembrane oligomeric intermediates of an α-helical toxin. *Langmuir.* 33:11496–11510.
21. Jo, S., T. Kim, …, W. Im. 2008. CHARMM-GUI: a web-based graphical user interface for CHARMM. *J. Comput. Chem.* 29:1859–1865.
22. Pronk, S., S. Páll, …, E. Lindahl. 2013. GROMACS 4.5: a high-throughput and highly parallel open source molecular simulation toolkit. *Bioinformatics.* 29:845–854.
23. Wang, J., R. M. Wolf, …, D. A. Case. 2004. Development and testing of a general Amber force field. *J. Comput. Chem.* 25:1157–1174.
24. Jämbeck, J. P. M., and A. P. Lyubartsev. 2012. Derivation and systematic validation of a refined all-atom force field for phosphatidylcholine lipids. *J. Phys. Chem. B.* 116:3164–3179.
25. Desikan, R., A. Behera, …, K. G. Ayappa. 2021. Using multiscale molecular dynamics simulations to obtain insights into pore forming toxin mechanisms. *Methods Enzymol.* 649:461–502.
26. Jämbeck, J. P. M., and A. P. Lyubartsev. 2012. An extension and further validation of an all-atomistic force field for biological membranes. *J. Chem. Theor. Comput.* 8:2938–2948.
27. Grote, F., and A. P. Lyubartsev. 2020. Optimization of slipids force field parameters describing headgroups of phospholipids. *J. Phys. Chem. B.* 124:8784–8793.
28. Hess, B., H. Bekker, …, J. G. E. M. Fraaije. 1997. LINCS: a linear constraint solver for molecular simulations. *J. Comput. Chem.* 18:1463–1472.
29. Parrinello, M., and A. Rahman. 1981. Polymorphic transitions in single crystals: A new molecular dynamics method. *J. Appl. Phys.* 52:7182–7190.
30. Branduardi, D., F. L. Gervasio, and M. Parrinello. 2007. From A to B in free energy space. *J. Chem. Phys.* 126, 054103.
31. Hedger, G., H. Koldsø, …, M. S. P. Sansom. 2019. Cholesterol interaction sites on the transmembrane domain of the hedgehog signal transducer and class FG protein-coupled receptor smoothened. *Structure.* 27:549–559.e2.
32. Koldsø, H., D. Shorthouse, …, M. S. P. Sansom. 2014. Lipid clustering correlates with membrane curvature as revealed by molecular simulations of complex lipid bilayers. *PLoS Comput. Biol.* 10, e1003911.
33. Allouche, A.-R. 2011. Gabedit—A graphical user interface for computational chemistry softwares. *J. Comput. Chem.* 32:174–182.
34. Yesylevskyy, S. O., and C. Ramseyer. 2014. Determination of mean and Gaussian curvatures of highly curved asymmetric lipid bilayers: the case study of the influence of cholesterol on the membrane shape. *Phys. Chem. Chem. Phys.* 16:17052–17061.
35. Agrawal, A., K. Apoorva, and K. G. Ayappa. 2017. Transmembrane oligomeric intermediates of pore forming toxin Cytolysin A determine leakage kinetics. *RSC Adv.* 7:51750–51762.
36. Vaidyanathan, M. S., P. Sathyanarayana, …, K. G. Ayappa. 2014. Lysis dynamics and membrane oligomerization pathways for Cytolysin A (ClyA) pore-forming toxin. *RSC Adv.* 4:4930–4942.
37. Miller, C. M., A. C. Brown, and J. Mittal. 2014. Disorder in cholesterol-binding functionality of CRAC peptides: A molecular dynamics study. *J. Phys. Chem. B.* 118:13169–13174.
38. Fantini, J., and F. J. Barrantes. 2013. How cholesterol interacts with membrane proteins: an exploration of cholesterol-binding sites including CRAC, CARC, and tilted domains. *Front. Physiol.* 4:31.
39. Plesnar, E., W. K. Subczynski, and M. Pasenkiewicz-Gierula. 2012. Saturation with cholesterol increases vertical order and smoothes the surface of the phosphatidylcholine bilayer: A molecular simulation study. *Biochim. Biophys. Acta.* 1818:520–529.
40. Ferreira, T. M., F. Coreta-Gomes, …, D. Topgaard. 2013. Cholesterol and POPC segmental order parameters in lipid membranes: solid state 1 H–13 C NMR and MD simulation studies. *Phys. Chem. Chem. Phys.* 15:1976–1989.
41. Pang, K. Y., and K. W. Miller. 1978. Cholesterol modulates the effects of membrane perturbers in phospholipid vesicles and biomembranes. *Biochim. Biophys. Acta.* 511:1–9.
42. Subczynski, W. K., M. Pasenkiewicz-Gierula, …, M. Raguz. 2017. High cholesterol/low cholesterol: effects in biological membranes: a review. *Cell Biochem. Biophys.* 75:369–385.

43. Ramakrishnan, N., R. P. Bradley, …, R. Radhakrishnan. 2018. Biophysics of membrane curvature remodeling at molecular and mesoscopic lengthscales. *J. Phys. Condens. Matter.* 30, 273001.

44. Chakraborty, H., and D. Sengupta. 2022. Preface to special issue on protein-mediated membrane remodeling. *J. Membr. Biol.* 255:633–635.

45. Pandit, S. A., S.-W. Chiu, …, H. L. Scott. 2008. Cholesterol packing around lipids with saturated and unsaturated chains: a simulation study. *Langmuir.* 24:6858–6865.

46. Duwe, H., J. Kaes, and E. Sackmann. 1990. Bending elastic moduli of lipid bilayers: modulation by solutes. *J. Phys. France.* 51:945–961.

47. Hofsäß, C., E. Lindahl, and O. Edholm. 2003. Molecular dynamics simulations of phospholipid bilayers with cholesterol. *Biophys. J.* 84:2192–2206.

48. Viswanathan, G., M. Jafurulla, …, A. Chattopadhyay. 2015. Dissecting the membrane cholesterol requirement for mycobacterial entry into host cells. *Chem. Phys. Lipids.* 189:19–27.